Russian Journal of Earth Sciences

Mathematical Model of Degradation of Frozen Hydrate-Bearing Saline Rocks under Thermal Influence from Above and Below

M. M. Ramazanov[1,2], L. I. Lobkovsky[3], N. S. Bulgakova[*,1,4], and S. R. Gadzhimagomedova[1,4]

[1] Institute for Geothermal Research and Renewable Energy of the Joint Institute for High Temperatures of the Russian Academy of Sciences, Makhachkala, Russia
[2] Institute of Geospheres Dynamics of Russian Academy of Sciences, Moscow, Russia
[3] Shirshov Institute of Oceanology, Russian Academy of Sciences, Moscow, Russia
[4] Dagestan State Institute of National Economy, Makhachkala, Russia
* Correspondence to: Natalia Bulgakova, ipgnatali@mail.ru

Abstract: A mathematical model has been formulated to describe the degradation of saline permafrost containing ice, gas hydrate accumulations, and free gas, as a result of climate warming and the influence of heat flow from below, considering the effects of osmosis. The degradation rates of hydrate-bearing permafrost from above and below, along with the corresponding rates of methane release into the surrounding permeable fractured-porous medium and gas migration channels or faults, have been studied. To investigate degradation from above, several temperature values at the upper boundary of the frozen layer were considered, including both positive and negative values in degrees Celsius. This allowed for the separate assessment of the contributions of heat and salinity to the degradation rates, as well as to evaluate the role of osmotic forces. To investigate degradation from below, several values of heat flow caused by the geothermal gradient were considered. As an application of the model, the results of calculations for the degradation rates of the frozen hydrate-bearing layer, following the onset of ocean transgression on the Arctic shelf approximately 10 thousand years ago, are presented.

Keywords: permafrost, gas hydrate, ice melting, degradation, solutions, osmosis, mathematical model

Citation: Ramazanov M. M., Lobkovsky L. I., Bulgakova N. S., and Gadzhimagomedova S. R. (2025), Mathematical Model of Degradation of Frozen Hydrate-Bearing Saline Rocks under Thermal Influence from Above and Below, *Russian Journal of Earth Sciences*, 25, ES5021, EDN: KSEZMC, https://doi.org/10.2205/2025es001031

Research Article

Received: March 20, 2025
Accepted: June 9, 2025
Published: November 17, 2025

Introduction

Global warming, driven by the presence of greenhouse gases in the atmosphere, is one of the most significant contemporary environmental issues [*Sergienko et al.*, 2012]. Anthropogenic activities are considered the primary source of these gases. Methane is the second most significant greenhouse gas after carbon dioxide. Although its atmospheric concentration is considerably lower than that of CO_2, the contribution of increasing atmospheric CH_4 to the greenhouse effect is estimated to be approximately 30% of that of carbon dioxide. This is because methane's radiative efficiency is 20–35 times higher, and its concentration is increasing at a rate roughly 2–4 times faster than that of CO_2 [*Semiletov and Shakhova*, 2024].

The Arctic is warming significantly faster than other regions of the planet. At the same time, intense methane emissions have been recorded on the Siberian Arctic shelf [*Lobkovskii et al.*, 2013]. It is now established that the primary source of atmospheric methane in the

Arctic region is the shelf of the Eastern Arctic seas, including the Laptev Sea, the East Siberian Sea, and the Russian sector of the Chukchi Sea. However, methane emissions may originate from multiple sources [*Yakushev*, 2009]: (1) the release of gaseous methane from gas hydrates, with large deposits identified on the Eastern Arctic shelf; (2) the release of methane previously trapped in permafrost as it thaws; and (3) the migration of endogenous methane through deep fault in rift zones.

Most submarine permafrost was formed on continental shelves during periods of low sea levels associated with major glacial events [*Osterkamp and Gosink*, 1991]. When glaciers melted around 10 000 years ago, sea levels rose, leading to the submergence of this permafrost [*Are et al.*, 2000]. Submergence can significantly alter permafrost properties, as it becomes exposed to overlying seawater, which can warm it by up to 17 °C [*Romanovskii et al.*, 2005].

Although relict permafrost gas hydrate deposits likely account for only a small portion of global hydrate reserves [*Ruppel*, 2011], they have recently attracted disproportionate attention due to their high sensitivity to climate change.

Although permafrost varies by the location, borehole records indicate a subsea permafrost base at a depth of 400–780 m [*Frederick and Buffett*, 2014]. In the cryolithozone, gas hydrates (mostly methane hydrates) typically exist at depths of 250 m, where the current hydrate stability zone begins [*Istomin and Yakushev*, 1992; *Yakushev et al.*, 2014]. However, recent field and laboratory studies suggest the possibility of relict gas hydrate deposits in the upper permafrost layers, at depths of up to 100–150 m. This is due to the effect of gas hydrate self-preservation at negative temperatures [*Chuvilin et al.*, 2019; *Yakushev*, 2009].

Bottom water temperatures are typically below 0 °C in the coastal zones of the Arctic Ocean. For example, in the Beaufort region of Alaska, the temperature of the bottom waters ranges from −0.5 °C to −1.7 °C, and in the Laptev Sea, temperatures can drop to −2 °C [*Osterkamp*, 2001]. However, in regions near river inflows (discharge zones), bottom water temperatures can reach 3 °C, as observed during summer near the Lena River delta on the East Siberian Arctic Shelf (ESAS) [*Shakhova et al.*, 2010]. In [*Frederick and Buffett*, 2014], a bottom water temperature of 0 °C is applied as a boundary condition when shelf sediments are submerged, reflecting the assumption that the area is adjacent to a modern river outflow.

In [*Shakhova et al.*, 2017], the results of direct observations of sediment temperatures in boreholes in the coastal zone of the Laptev Sea are presented. According to the obtained data, sediment temperatures ranged from −3 °C to +1 °C, with increases observed in some cores.

Since field research in the Arctic is difficult to conduct, theoretical studies based on mathematical modeling have come to the forefront.

Mathematical modeling of the processes of rock degradation (or freezing) and gas hydrate decomposition under various conditions has been the focus of numerous studies [*Harrison and Osterkamp*, 1976; *Lobkovsky et al.*, 2022; *Malakhova and Golubeva*, 2016; *Ramazanov et al.*, 2024a; *Tsypkin*, 2009; *Vasiliev et al.*, 1996]. For example, [*Harrison and Osterkamp*, 1976] and [*Malakhova and Golubeva*, 2016] examine permafrost degradation. However, these models rely on diffusion equations and do not account for the influence of convective transport heat and salt. A relatively similar model is discussed in [*Frederick and Buffett*, 2014], where both salt transport and heat transfer are considered, but it focuses solely on the decomposition of stable (deep) gas hydrates along with ice melting. Interestingly, tectonic waves may act as a trigger for the massive methane emissions from frozen sedimentary deposits into the atmosphere [*Lobkovsky et al.*, 2023; *Lobkovsky and Ramazanov*, 2021].

It is important to note that none of the known models of permafrost degradation take osmosis into account. Osmotic effects occur in clayey and silty low-permeability sediments saturated with solutions of inhomogeneous salt concentrations [*Ramazanov*, 2023; *Ramazanov et al.*, 2025a, 2019].

The osmotic effect is accounted for in our previous studies investigating the freezing of solution-saturated rocks [*Ramazanov et al.*, 2023; *Ramazanov et al.*, 2024b]. These studies have shown that during freezing, a significant part of the salt is adsorbed in frozen rocks, while the other part is displaced downward by the freezing front, and under certain conditions cryopegs (lenses and layers of highly mineralized waters with negative temperatures) can form in the permafrost. This is consistent with modern ideas that, during geological history, the rock strata in the coastal zone of the Siberian Arctic shelf were subject to periodic freezing and thawing processes. As a result, saline frozen rocks with a large number of cryopegs formed here [*Shakhova et al.*, 2010; *Streletskaya and Leibman*, 2002]. When saline frozen rocks thaw, the salt dissolves in the resulting moisture, increasing the concentration of the solution and, thus, enhancing the osmotic effect.

One of the main objectives of this study is to identify and compare the patterns of permafrost degradation from above and below, on the one hand, and to identify and compare the contribution of factors such as heat, salt, osmotic effect, etc. to the rates of permafrost and hydrate degradation, on the other hand.

Problem Formulation

The system under study is a saline permafrost layer – an impermeable frozen zone containing ice, metastable gas hydrates, and immobile accumulations of free gas (Figure 1). The initial conditions are defined such that the temperature within the layer increases linearly with depth, ranging from 251 K at the upper boundary to 273 K at the lower boundary. A geothermal gradient (heat flux) G is specified at the lower boundary. At time $t = t_0$, the temperature at the upper boundary of the layer sharply increases to T_0 and remains constant thereafter. We will study the process of bidirectional degradation of the frozen layer from both above and below, accompanied by gas hydrate decomposition and gas release through discharge channels.

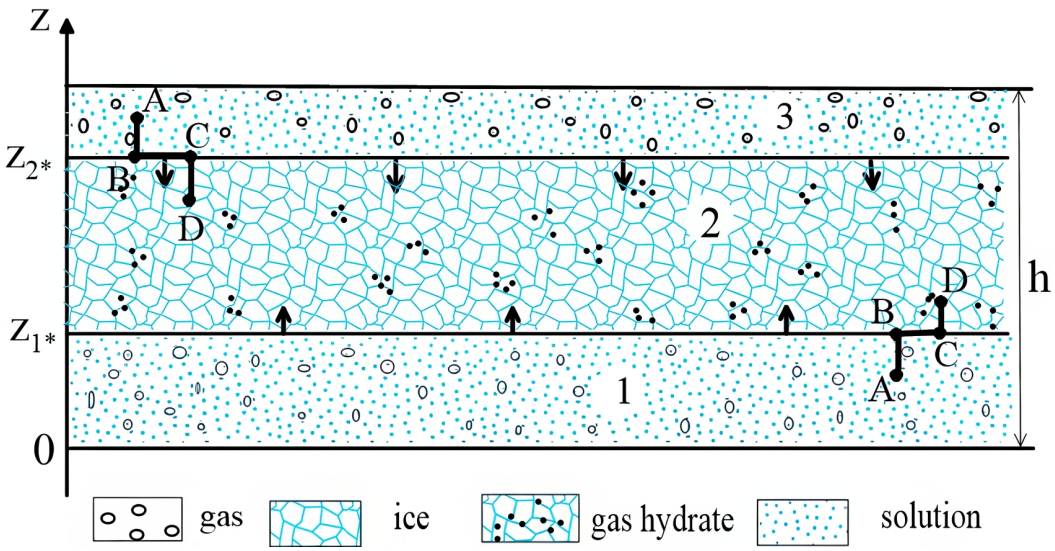

Figure 1. Problem sketch: 1,3 – thawed domain saturated with salt solution and free gas; 2 – impermeable frozen domain, containing ice, stable or metastable gas hydrate and accumulations of free gas; $z = z_{1*}(t)$ – degradation front from below; $z = z_{2*}(t)$ – degradation front from above.

Mathematical model

We present the systems of equations for each domain and the boundary conditions at the phase boundaries. The z-axis is directed upward, and the coordinate system is chosen as shown in Figure 1.

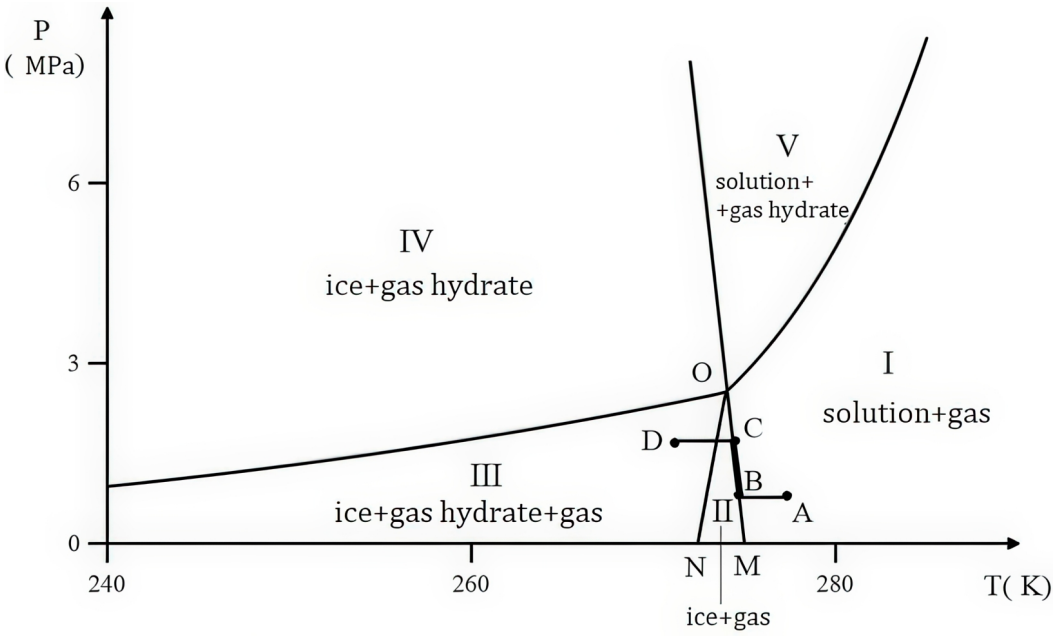

Figure 2. Thermodynamic diagram for the system ice + gas hydrate. Point O represents the quadruple point. The gas hydrate is metastable in domain III and stable in domains IV and V. Points A, B, C, and D correspond to those in Figure 1. Crossing boundary ON (left to right) causes the self-preserved gas hydrate to decompose; crossing boundary OM leads to ice melting.

Domains 1 and 3. In these domains, the rocks are saturated only with liquid solution and free gas. The system of equations in the thawed domain can be written as:

$$
\begin{aligned}
&v_w = -\tfrac{kf_w(s_w)}{\eta_w}\Big(\rho_w \tfrac{\partial \mu_1}{\partial c} c' + p' + \rho_w g\Big), && v_g = -\tfrac{kf_g(s_g)}{\eta_g}\Big(p' + \rho_g g\Big) \\
&\tfrac{\partial}{\partial t}(m s_w \rho_w) + (\rho_w v_w)' = 0, && \rho_w = \rho_w(p, T, c) \\
&\tfrac{\partial}{\partial t}\Big(m s_g \rho_g\Big) + \Big(\rho_g v_g\Big)' = 0, && \rho_g = \rho_g(p, T, c) \\
&(m s_w + \Gamma)\tfrac{\partial c}{\partial t} + v_w c' = (s_w D c')', && \Gamma(K, c) = \tfrac{\partial a(K,c)}{\partial c}, \qquad \lim_{Kc \to \infty} a(K, c) = a_\infty \\
&C_m \tfrac{\partial T}{\partial t} + \Big(\rho_w C_w v_w + \rho_g C_p v_g\Big) T' = (\lambda_m T')' \\
&C_m = m\Big(s_w \rho_w C_w + s_g \rho_g C_p\Big) + (1 - m) C_s, && \lambda_m = m\Big(s_w \lambda_w + s_g \lambda_g\Big) + (1 - m)\lambda_s
\end{aligned}
\tag{1}
$$

Here and below, we use the following notation: the prime means the derivative with respect to z; m is the layer porosity; k is the layer permeability; s_w, s_i, s_h, s_g are the saturations of the layer with solution, ice, gas hydrate and gas, respectively; $f_w(s_w)$, $f_g(s_g)$ are phase permeabilities of the solution and gas; ρ_w, ρ_i, ρ_h, ρ_g are the densities of the solution, ice, hydrate and gas, respectively; v_w, v_g are filtration velocity fields of the solution and gas, respectively; C_m is the effective heat capacity of a unit volume of a saturated porous medium; C_w, C_i, C_p, C_s are the specific heat capacities of the solution, ice, gas and rock matrix, respectively; T is the temperature; p is the pressure; c is the concentration of salt in the solution; c_0 is the characteristic concentration; λ_m is the effective thermal conductivity of a saturated porous medium; λ_w, λ_i, λ_g, λ_s are the thermal conductivities of the solution, ice, gas, and rocks; μ_1 is the chemical potential of the solvent in the solution; η_w, $\eta_g$are the viscosities of solution and gas; D is the diffusion coefficient of salt in solution; q is specific heat of ice melting; a is the concentration of salt in the solid phase of the porous medium; K-adsorption equilibrium constant; β_w, β_g are the coefficients of thermal expansion of solution and gas.

Domain 2. In this frozen domain, the medium is immobile; therefore, only the heat conduction equation applies here:

$$\begin{aligned} &C_{mi}\frac{\partial T}{\partial t} = \lambda_{mi}T'', \\ &C_{mi} = m\Big(\rho_i s_{i0}C_i + \rho_h s_{h0}C_h + \rho_g s_{g0}C_g\Big) + (1-m)C_s, \\ &\lambda_{mi} = m\Big(\rho_i s_{i0}\lambda_i + \rho_h s_{h0}\lambda_h + \rho_g s_{g0}\lambda_g\Big) + (1-m)\lambda_s. \end{aligned} \tag{2}$$

Here s_{h0} and $s_{i0} = 1 - s_{h0}$ are characteristic hydrate saturation and ice saturation in the frozen domain, C_{mi}, $\lambda_{mi}$are the effective heat capacity and thermal conductivity of a porous medium saturated with ice, preserved hydrate and immobile gas.

Note, in general, this frozen ice-saturated domain may contain small amounts of unfrozen water with dissolved salt ions. However, due to their small quantities, their influence on the thermal conductivity coefficient can be neglected.

Boundary conditions:

$$z = 0 \quad : T' = -G, \qquad p = p_1^0, \qquad c = c_1^0, \tag{3}$$

$$\begin{aligned} z = z_{1^*} : &\rho_w(v_w - ms_w\dot{z}_{1^*})_- = -\Big(\rho_i s_{i0} + \gamma\rho_h s_{h0}\Big)m\dot{z}_{1^*}, \\ &\rho_g\Big(v_g - ms_g\dot{z}_{1^*}\Big)_- = -(1-\gamma)\rho_h s_{h0}m\dot{z}_{1^*}, \\ &T_- = T_+ = T_{1^*}, \qquad -\lambda_- T'_- - qm\Big(\rho_i s_{i0} + \gamma\rho_h s_{h0}\Big)\dot{z}_{1^*} = -\lambda_+ T'_+, \\ &c = c_0, \qquad p_{1^*} = F(T_{1^*}, c_0), \end{aligned} \tag{4}$$

$$\begin{aligned} z = z_{2^*} : &\rho_w(v_w - ms_w\dot{z}_{2^*})_- = -\Big(\rho_i s_{i0} + \gamma\rho_h s_{h0}\Big)m\dot{z}_{2^*}, \\ &\rho_g\Big(v_g - ms_g\dot{z}_{2^*}\Big)_- = -(1-\gamma)\rho_h s_{h0}m\dot{z}_{2^*}, \\ &T_- = T_+ = T_{2^*}, \qquad -\lambda_- T'_- - qm\Big(\rho_i s_{i0} + \gamma\rho_h s_{h0}\Big)\dot{z}_{2^*} = -\lambda_+ T'_+, \\ &c = c_0, \qquad p_{2^*} = F(T_{2^*}, c_0), \end{aligned} \tag{5}$$

$$z = h \quad : T = T_3^0, \qquad p = p_3^0, \qquad c = c_3^0 \tag{6}$$

Here and below, γ is the mass fraction of water molecules in the gas hydrate. The subscripts are defined as follows: the subscript '+' refers to the value of the quantity when approaching the boundary from below, the subscript '–' refers to the value when approaching from above, and the subscript '*' denotes the value at the boundary $z = z_*$. The system of equations (1–6) with the initial conditions, forms a closed mathematical model for solving the problem.

Note that the pressure boundary conditions in (3) and (6) can be replaced by impermeability conditions, either on both boundaries or on one of them, if required.

Let's make two important points.

1. As indicated in the problem statement, the initial conditions are such that the reservoir temperature increases linearly with depth from a value of 251 at the upper boundary of the reservoir to 273 at its lower boundary. This distribution was chosen based on several considerations. Before the transgression of the sea, rocks on the upper permafrost boundary have a very low temperature due to long-term contact with cold air. On the other hand, it is known that the temperature of rocks increases with depth and it is clear that, starting from a certain depth, there is no permafrost. The simplest function that takes these conditions into account is a linear distribution. On the other hand, the direct calculation of permafrost formation starting from the last glacial

cycle about 130 thousand years ago, according to [*Frederick and Buffett*, 2014], by the beginning of the transgression leads to a close distribution, considered here as the initial one. Finally, the linear temperature distribution is a quasi-stationary solution to the thermal problem in permafrost at the initial time before the occurrence of disturbances.

2. This model considers one front of permafrost degradation from above and one front below. In fact, during the degradation of permafrost containing gas hydrates, not one mobile front appears, but two [*Ramazanov et al.*, 2025b], for example, during the decomposition of preserved relict gas hydrates. Generally speaking, these fronts of gas hydrate degradation and ice melting do not coincide. And each of them should have its own latent heat of the phase transition. Taking this fact into account would lead to a severe complication of an already difficult task. At the same time, the results would not have changed much [*Ramazanov et al.*, 2025b]. Therefore, at the first stage, it was assumed that these two fronts coincide, and the heats of phase transitions can be effectively accounted for using a single q value under boundary conditions (4–5).

Quasi-self-similar formulation and solution of the problem. As shown in [*Ramazanov et al.*, 2023], in the considered problems, hydrostatics can be neglected in the first approximation, which allows the equations to be written in a self-similar or quasi-self-similar form, depending on the boundary and initial conditions.

In studying permafrost degradation rates, it is convenient to divide this problem into two, upper and lower. These problems can be considered independently until the fronts approach sufficiently, i.e. for almost the entire time interval of main interest. The upper problem (degradation from above) has been thoroughly examined in our previous works, where we considered the frozen, thawed, and transition domains [*Ramazanov et al.*, 2025b]. Here, we analyze both problems from a unified perspective.

We write the problem in a dimensionless form by introducing the following scales

$$\begin{aligned} &[z]=h, \qquad [v]=\tfrac{k}{\eta h}[p], \qquad [t]=\tfrac{h}{[v]}, \qquad [T]=T_3^0-T_0, \\ &[p]=\tfrac{dP_*}{dT}\Big(T_3^0-T_0\Big), \qquad [c]=c_0. \end{aligned} \tag{7}$$

and notations

$$\begin{aligned} &\beta_{pw}=s_{w0}m\Big(\tfrac{1}{m}\tfrac{\partial m}{\partial p}+\tfrac{1}{\rho_w}\tfrac{\partial \rho_w}{\partial p}\Big)[p], \qquad \beta_{pg}=s_{g0}m\Big(\tfrac{1}{m}\tfrac{\partial m}{\partial p}+\tfrac{1}{\rho_g}\tfrac{\partial \rho_g}{\partial p}\Big)[p], \\ &\gamma_f=\rho_w\tfrac{\partial \mu_1}{\partial c}c_0[p]^{-1}, \qquad \gamma_c=ms_{w0}+\Gamma, \qquad \gamma_T=\tfrac{C_m}{\rho_w C_w}, \qquad \gamma_q=\tfrac{qm\rho_i}{\rho_w C_w[T]}, \\ &Pe_T=\tfrac{[v]h\rho_w C_w}{\lambda_m}, \qquad Pe_c=\tfrac{[v]h}{ms_{w0}D}, \qquad [v]=\tfrac{k}{\eta h}[p]. \end{aligned} \tag{8}$$

Here, s_{w0} and $s_{g0}=1-s_{w0}$ are the characteristic water saturation and gas saturation in the thawed domain.

1. Degradation from below

We will seek the solution in a quasi-self-similar form by introducing a new coordinate ξ:

$$v=\frac{v(\xi,t)}{\sqrt{t}}, \qquad T=T(\xi,t), \qquad c=c(\xi,t), \qquad p=p(\xi,t), \qquad \xi=\frac{z}{\sqrt{t}}. \tag{9}$$

Then, assuming $(\partial/\partial t)_\xi=0$ for all fields in domains 1 and 2, we obtain:
In thawed domain 1

$$\begin{aligned} &v_w=s_w\Big(-p'+\gamma_f c'\Big), \qquad v_g=-s_g\tfrac{\eta_w}{\eta_g}p', \\ &-\tfrac{\xi}{2}\Big(ms_w'-\beta_{pw}p'\Big)+v_w'=0, \qquad -\tfrac{\xi}{2}\Big(ms_g'-\beta_{pg}p'\Big)+v_g'=0, \\ &-\Big(\tfrac{\gamma_c\xi}{2}-v_w\Big)c'=\tfrac{1}{Pe_c}c'', \\ &-\Big(\tfrac{\gamma_T\xi}{2}-v_w-\tfrac{\rho_g C_p}{\rho_w C_w}v_g\Big)T'=\tfrac{1}{Pe_T}T''. \end{aligned} \tag{10}$$

In frozen domain 2

$$-\frac{\xi}{2}T' = \frac{1}{Pe_{Ti}}T'', \tag{11}$$

where

$$Pe_{Ti} = \frac{[v]hC_{mi}}{\lambda_{mi}}, \qquad [v] = -\frac{k}{\eta_w h}[p]. \tag{12}$$

Boundary conditions in self-similar coordinates

$$\begin{array}{ll}
\xi = 0: & T' = -\sqrt{t}G, \quad p = p_1^0, \quad c = c_1^0, \\
\xi = \xi_{1^*}(t): & \rho_w\left(v_w - ms_w\sqrt{t}\dot{z}_{1^*}\right)_- = -\left(\rho_i s_{i0} + \gamma\rho_h s_{h0}\right)m\sqrt{t}\dot{z}_{1^*}, \quad z_{1^*} = \xi_{1^*}(t)\sqrt{t}, \\
& \rho_g\left(v_g - ms_g\sqrt{t}\dot{z}_{1^*}\right)_- = -(1-\gamma)\rho_h s_{h0}m\sqrt{t}\dot{z}_{1^*}, \\
& T_- = T_+ = T_{1^*}, \quad -\frac{1}{Pe_{T-}}T'_- - \gamma_q\left(\rho_i s_{i0} + \gamma\rho_h s_{h0}\right)\sqrt{t}\dot{z}_{1^*} = -\frac{1}{Pe_{T+}}T'_+, \\
& c = c_0, \quad p_{1^*} = F(T_{1^*}, c_0), \\
\xi = \infty: & T \to T_0.
\end{array} \tag{13}$$

2. Degradation from above

As before, we will seek the solution in a quasi-self-similar form by introducing a new coordinate ξ

$$v = \frac{v(\xi,t)}{\sqrt{t}}, \quad T = T(\xi,t), \quad c = c(\xi,t), \quad p = p(\xi,t), \quad \xi = \frac{h-z}{\sqrt{t}}. \tag{14}$$

Equations (14) differ from (9) in that the axis 0ξ now starts at the upper boundary and is directed downward. Then we obtain:

In thawed domain 3

$$\begin{array}{l}
v_w = s_w\left(-p' + \gamma_f c'\right), \quad v_g = -s_g\frac{\eta_w}{\eta_g}p', \\
-\frac{\xi}{2}\left(ms'_w - \beta_{pw}p'\right) + v'_w = 0, \quad -\frac{\xi}{2}\left(ms'_g - \beta_{pg}p'\right) + v'_g = 0, \\
-\left(\frac{\gamma_c\xi}{2} - v_w\right)c' = \frac{1}{Pe_c}c'', \\
-\left(\frac{\gamma_T\xi}{2} - v_w - \frac{\rho_g C_p}{\rho_w C_w}v_g\right)T' = \frac{1}{Pe_T}T''.
\end{array} \tag{15}$$

In frozen domain 2

$$-\frac{\xi}{2}T' = \frac{1}{Pe_{Ti}}T''. \tag{16}$$

Boundary conditions in self-similar coordinates

$$\begin{array}{ll}
\xi = 0: & T = T_3^0, \quad p = p_3^0, \quad c = c_3^0, \\
\xi = \xi_{2^*}: & \rho_w\left(v_w - ms_w\frac{\xi_{2^*}}{2}\right)_- = -\left(\rho_i s_{i0} + \gamma\rho_h s_{h0}\right)m\frac{\xi_{2^*}}{2}, \\
& \rho_g\left(v_g - ms_g\frac{\xi_{2^*}}{2}\right)_- = -(1-\gamma)\rho_h s_{h0}m\frac{\xi_{2^*}}{2}, \\
& T_- = T_+ = T_{2^*}, \quad -\frac{1}{Pe_{T-}}T'_- - \gamma_q\left(\rho_i s_{i0} + \gamma\rho_h s_{h0}\right)\frac{\xi_{2^*}}{2} = -\frac{1}{Pe_{T+}}T'_+, \\
& c = c_0, \quad p_{2^*} = F(T_{2^*}, c_0), \\
\xi = \infty: & T \to T_0.
\end{array} \tag{17}$$

The equations (2–6), and in self-similar coordinates (9–17), represent a closed mathematical model of the degradation of frozen rocks containing ice, gas hydrates, and immobile gas accumulations under thermal and saline influences from below and above, taking into account osmosis and rock deformation.

Solution Method. In the frozen domain 2, an exact solution to the heat conduction equation is obtained. In domains 1 and 3, the solution is found numerically. These solutions are then matched at the boundaries using the boundary conditions. For numerical calculations,

a generalized variable $Q = v_w + (\eta_g/\eta_w)v_g$ is introduced to reformulate the problem as a first-order system solvable with respect to the derivatives. The system is then solved iteratively using a finite difference method, with the number of iterations and grid points chosen to ensure convergence and accuracy. The physical validity of the results is confirmed by their agreement with experimental data.

Discussion

The primary objective of this work was to establish a mathematical model for analyzing the degradation rates and mechanisms of a frozen hydrate-bearing layer, accounting for the osmotic effect. The degradation of the frozen stratum from above is caused by a temperature jump resulting from the transgression of the sea on the Arctic shelf ten thousand years ago, and from below by a heat flow associated with a geothermal temperature gradient. Calculations were performed for the following parameter values: $R = 8.3\,\text{J/(K·mol)}$, $\rho_w = 10^3\,\text{kg/m}^3$, $\rho_i = 0.92 \times 10^3\,\text{kg/m}^3$, $\rho_h = 0.9 \times 10^3\,\text{kg/m}^3$, $s_{h0} = 0.8$, $s_{i0} = 0.2$, $\gamma_h = 0.87$, $T^0 = (272; 273.2 \text{ and } 274)\,\text{K}$, $q = (50; 60 \text{ and } 80)\,\text{mW/m}^2$, $(c^0, c_0) = (6, 20), (0.1, 1)\,\text{g/L}$, $h = 700\,\text{m}$, $m = 0.3$, $k = 10^{-16}\,\text{m}^2$, $\eta_w = 1.8{\times}10^{-3}\,\text{Pa·s}$, $\eta_g = 10^{-5}\,\text{Pa·s}$, $D = 10^{-9}\,\text{m}^2/\text{s}$, $C_s = 1.38\,\text{kJ/(kg·K)}$, $C_h = 2.08\,\text{kJ/(kg}\cdot\text{K)}$, $C_i = 2.09\,\text{kJ/(kg}\cdot\text{K)}$, $C_g = 2.23\,\text{kJ/(kg}\cdot\text{K)}$, $C_w = 4.18\,\text{kJ/(kg}\cdot\text{K)}$, $\lambda_s = 5.5\,\text{W/(m}\cdot\text{K)}$, $\lambda_h = 0.5\,\text{W/(m}\cdot\text{K)}$, $\lambda_i = 2.18\,\text{W/(m}\cdot\text{K)}$, $\lambda_q = 0.03\,\text{W/(m}\cdot\text{K)}$, $\lambda_w = 0.58\,\text{W/(m}\cdot\text{K)}$.

As noted earlier, these problems can be treated independently over most of the time interval of interest. We present the results for degradation from above and below separately and compare corresponding degradation rates.

Degradation of hydrate-bearing permafrost from above. The initial conditions are defined such that the temperature within the layer increases linearly with depth, ranging from 251 K at the upper boundary to 273 K at the lower boundary. At time $t = t_0$, the temperature at the upper boundary of the layer abruptly increases to T_0 and remains constant thereafter. Calculations were performed for the three different temperatures at the upper boundary $T^0 = (272; 273.2 \text{ and } 274)\,\text{K}$. These cases are labeled (1, 2, 3). For the convenience of presenting the results in the case under consideration (degradation from above), the z-axis is directed downward (in contrast to the Figure 1). Accordingly, the boundary conditions (6), which according to Figure 1 were set at $z = h$, correspond to the coordinate $z = 0$ in Figures 3–6.

Regarding the salt concentration during degradation from above, it was assumed that the frozen rocks are initially saline, and as the ice melts, the salt is released into the solution. In all cases (1, 2, 3), the salt concentration at the ice melting front was set to 20 g/L, while a lower concentration of 6 g/L was specified at the upper boundary of the thawed region. For degradation from below, different salt concentration values were considered.

Osmotic properties arise in the presence of a semipermeable membrane separating solutions of different salt concentrations [*Osterkamp*, 2001]. In nature, low-permeability clayey and silty rocks act as membranes, exhibiting osmotic properties [*Tsypkin*, 2009]. The permeability of clays is typically from 10^{-16} to $10^{-18}\,\text{m}^2$ or less [*Lobkovsky et al.*, 2022]. For the calculations, a permeability of $10^{-16}\,\text{m}^2$ was used.

Figure 3 illustrates case 1, where the boundary temperature is negative in degrees Celsius. In Figure 3a, osmosis is absent, i.e., $\gamma_f = 0$. The horizontal dashed line indicates the permafrost degradation front. The upper part of the figure presents the distributions of pore saturation by different phases in the thawed domain for various values of the osmotic coefficient after 1000 years from the start of the process. As shown in the figure, under the given conditions, the fractions of pore volume occupied by gas and liquid are comparable. An increase in the osmotic coefficient leads to a rise in pressure, resulting in gas compression and a reduction in gas saturation (is the fraction of pores occupied by gas).

Thus, gas can occupy a significant fraction of the pore volume, comparable to the volume occupied by water, due to the high gas pressure resulting from gas hydrate dissociation in the formation.

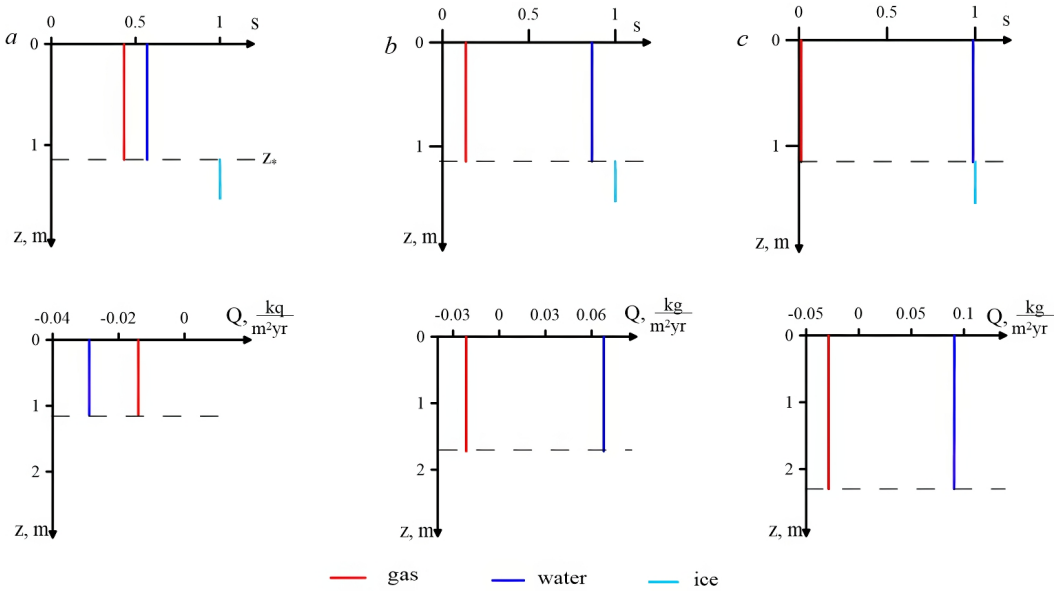

Figure 3. Distributions of pore saturation by different phases in the thawed domain 1000 years after the start of the permafrost degradation process (top row) for various values of the osmotic coefficient: $\gamma_f = 0; 10^{-5}$ and $10^{-4}(a, b, c)$; mass fluxes of gas and water in the thawed domain 1000 years after the start of the process (bottom row) for various values of the osmotic coefficient: $\gamma_f = 0; 7.5 \times 10^{-3}$ and $15 \times 10^{-3}(a, b, c)$.

The lower panel of Figure 3a illustrates the mass flux distributions of gas and water with depth in the thawed domain after 1000 years of degradation. In the absence of osmosis, the fluxes are negative, i.e., directed upward and discharged through the upper boundary of the thawed domain. This is because the pressure at the phase transition boundary is greater than that at the upper boundary of the thawed domain, resulting in a downward pressure gradient.

Figure 3b, c show cases, where osmotic coefficients are nonzero. Osmosis leads to a decrease in the fraction of pores occupied by gas in the thawed domain. This is because the gas is compressed due to an increase in pressure caused by osmosis, as shown in Figure 4a. The lower panels of Figure 3b, c demonstrate that as the osmotic force increases, the water flux reverses direction at a critical osmotic coefficient value, becoming positive (i.e., moving toward the phase transition front). This occurs because the concentration gradient in the thawed domain is positive in this case, causing the osmotic force to draw moisture downward toward the phase boundary, despite the opposing pressure gradient. With further increases in the osmotic coefficient, the magnitude of the water flux grows. In contrast, the gas flux direction remains unchanged, directed upward toward the discharge boundary. At the same time, the gas flux magnitude increases with osmotic force due to the rising pressure gradient (Figure 4a).

Figure 4 shows that osmosis leads to a significant increase in pressure and its gradient in the thawed domain. The pressure increase is caused by the osmotic influx of moisture into the transition zone. As the permeability of the layer (Péclet number) decreases and the initial salt concentration in the frozen rocks increases, pressure values can rise several times further, potentially leading to layer destruction [*Neuzil*, 2000].

Thus, if the osmotic coefficient is sufficiently large and the permeability is sufficiently low, significant stresses can develop in the saline layer due to osmosis, potentially leading to layer failure. This, in turn, may cause a rapid pressure drop, resulting in additional gas hydrate decomposition. This scenario is discussed in [*Morgado et al.*, 2024] as part of a possible mechanism for the formation and explosion of methane emission craters on the Yamal and Taimyr peninsulas in Siberia. As shown in [*Ramazanov et al.*, 2025a], if the concentration gradient is opposite, i.e. the concentration of salt solution above the

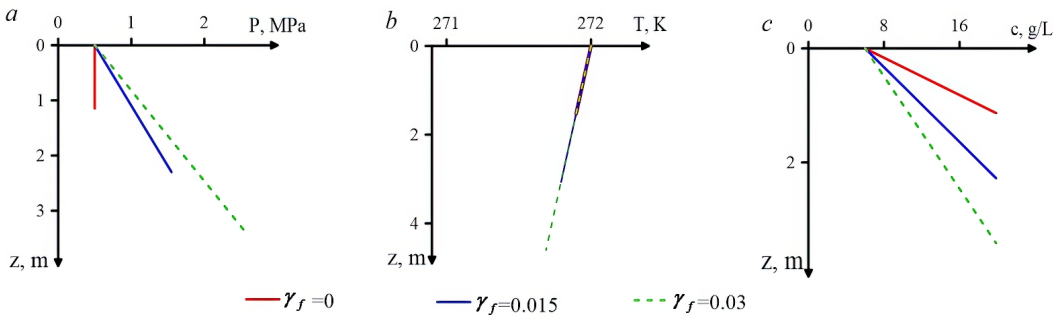

Figure 4. Distributions of pressure (a), temperature (b), and salt concentration (c) with depth 1000 years after the start of the process for various values of the osmosis coefficient: $\gamma_f = 0$; 1.5×10^{-2} and 3×10^{-2}.

formation is higher than within the rocks, then the osmotic force, on the contrary, tends to push the solution out of the thawed domain, which leads to pressure depression. It should be noted that earlier possible mechanisms of formation of gas emission craters, as well as the results of field studies and numerical experiments, were discussed in [*Arzhanov et al.*, 2020; *Bogoyavlensky*, 2021; *Kizyakov et al.*, 2017].

As shown in Figure 4, the temperature changes only slightly with an increase in the osmotic coefficient, while the salt concentration and its gradient in the thawed domain decrease, which is associated with an increase in the rate of permafrost degradation. Despite the decreasing salt concentration gradient ∇c, the osmotic force increases with the osmotic coefficient γ_f and equals the product of these values $\gamma_f \nabla c$.

The analyzed figures indicate that over 1000 years, the permafrost degradation front advances by only about one meter. On the one hand, this is because the temperature remains negative, and degradation occurs solely due to salt. On the other hand, the initial temperature of the upper part of the frozen layer is too low 251 K (−22 °C) for this salt concentration. For other cases where the boundary temperature is positive, the dependencies shown in Figures 3–4 remain qualitatively similar. However, as will be shown below, the degradation front advances 20–30 times farther. The combined influence of salt and heat on the layer degradation can be comparable, as observed in the case 3 at $T^0 = 274$ K, where the contribution of salt is approximately 55%. In the second case at $T^0 = 273.2$ K, the influence of salt is dominant; in its absence, degradation driven solely by heat is approximately 8 times slower.

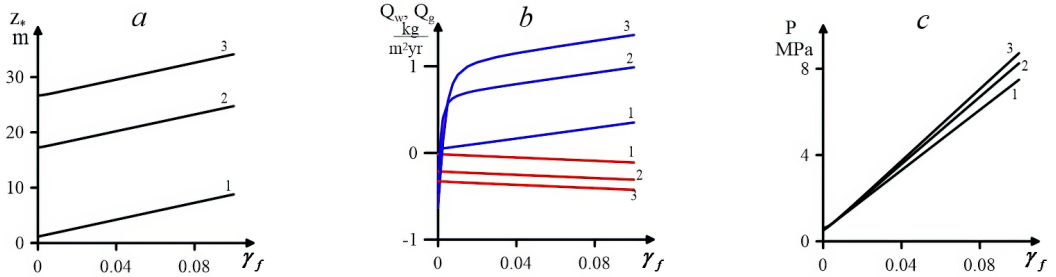

Figure 5. Dependence of the permafrost degradation front (a), the mass flux of gas and water (b), and the pressure at the phase transition boundary (c) on the dimensionless osmotic coefficient 1000 years after the onset of the process. Notation: lines 1 correspond to the case when the temperature at the upper boundary is 272 K, lines 2 – 273.2 K, lines 3 – 274 K; red lines – gas, blue – water.

Figure 5a–c illustrate the dependence of various parameters on the osmotic coefficient for all three cases 1000 years after the start of permafrost degradation. As shown in Figure 5a, osmosis increases the rate of degradation in frozen saline deposits. The largest relative contribution of osmosis is observed in the first case, where the temperature $T^0 = 272$ K is negative in Celsius, and degradation occurs solely due to the presence of salt.

In this scenario, degradation progresses from slightly more than one meter over 1000 years in the absence of osmosis to more than 8 meters with a significant osmotic effect. In cases 2 and 3, the temperature at the upper boundary is positive $T^0 = 273.2\,\mathrm{K}$ and $T^0 = 274\,\mathrm{K}$, respectively. In these cases, heat also influences the degradation process. For example, in case 3, even without osmosis, degradation reaches a depth of nearly 30 meters.

Figure 5b shows the dependence of gas and water fluxes through the upper boundary of the thawed domain discharge on the osmotic coefficient after 1000 years after the start of the process for all the considered cases. As seen in the figure, the gas flux ranges from several tens of $\mathrm{g/(m^2\,yr)}$ in case 1 to several hundred $\mathrm{g/(m^2\,yr)}$ in case 3. At the same time, osmosis can significantly increase the gas flux. Its effect on the water flux can be substantial not only quantitatively but also qualitatively. At low values of the osmotic coefficient, the water flux is directed upward, opposite to the movement of the degradation front, and ranges from tens to hundreds of $\mathrm{g/(m^2\,yr)}$ depending on the case. When the osmotic coefficient reaches a critical value, the water flux reverses direction (moving in the same direction as the degradation front) and can exceed $1000\,\mathrm{g/(m^2\,yr)}$ at high values of γ_f.

Figure 5c illustrates the dependence of water and gas pressure near the degradation front on the osmotic coefficient γ_f. As seen in the figure, osmosis can significantly increase pressure, reaching values of approximately 10 MPa, which is consistent with experimental data [*Neuzil*, 2000].

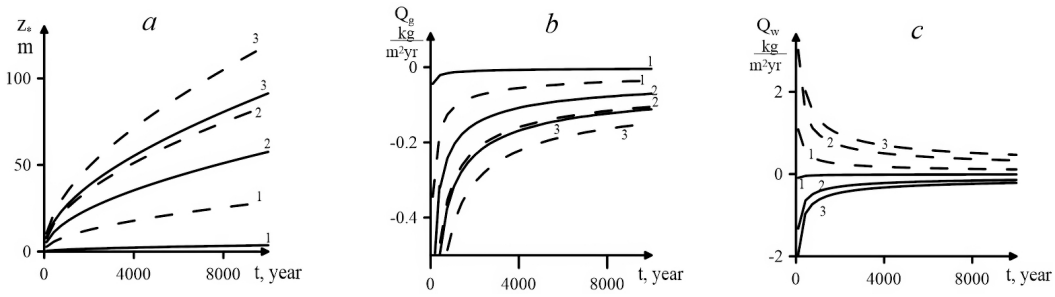

Figure 6. Dependence of the permafrost degradation front from above (a), gas flux (b), and water flux (c) on time for all cases. Notation: lines 1 correspond to the case when the temperature at the upper boundary is 272 K, lines 2 – 273.2 K, lines 3 – 274 K; solid lines correspond to the absence of osmosis, while dashed lines account for the influence of osmosis at $\gamma_f = 0.1$.

Figure 6 shows the time evolution of various parameters over ten thousand years, with and without the osmotic effect, illustrating their changes from approximately the time of the Arctic shelf marine transgression to the present for all three cases. Solid lines represent cases without osmosis, while dashed lines correspond to cases with an osmotic coefficient $\gamma_f = 0.1$. Figure 6a displays curves indicating the rates of permafrost degradation for different temperatures at the upper boundary. Figure 6b and c show the temporal changes in gas and water fluxes, respectively. The final values after 10 000 years, corresponding to Figure 6, are summarized in Table 1.

Table 1. Depth of degradation of hydrate-bearing permafrost from above and gas/water fluxes across the discharge boundary for different boundary temperatures, with and without the osmotic effect, after 10 000 years after the start of the process. Cases with osmosis at $\gamma_f = 0.1$are shown in parentheses

$T^0(K)$	272	273.2	274
$Z_*(m)$	3.6(28.6)	57.8(84)	91(119)
$Q_g\left(\frac{\mathrm{kg}}{\mathrm{m^2\cdot yr}}\right)$	−0.0045(−0.036)	−0.07(−0.1)	−0.11(−0.15)
$Q_w\left(\frac{\mathrm{kg}}{\mathrm{m^2\cdot yr}}\right)$	−0.01(0.1)	−0.14(0.33)	−0.22(0.47)

We compare two estimates resulting from the model with field experimental data. In [*Shakhova et al.*, 2017], experimental methods showed that permafrost degradation from above in the East Siberian Arctic Shelf coastal zone was observed at an average rate of 14.0 ± 3.1 cm/yr over 32 years (1982–2014). Data from [*Sergienko et al.*, 2012; *Shakhova et al.*, 2017] also suggest that methane flux through bottom sediments at the end of this period (after 31 years) can reach approximately 200 g/(m^2 yr).

For simplicity, we assume that the permafrost degradation process nominally began in 1982. We estimate these quantities using the obtained solution. According to (14), the distance (m) traveled by the degradation front from above over time t (yr) and the average rate (m/yr) of permafrost degradation are approximately equal to

$$z_{2^*} = C_2\sqrt{t}, \qquad v_* = \frac{C_2}{\sqrt{t}}. \tag{18}$$

In Table 1, we examine the second case, where $T^0 = 273.2$ K. By substituting $t = 10^4$ yr, $Z_{2^*} = 57.8(84)$ m into (18), we obtain $C_2 = 0.578(0.84)$.

According to (18), the permafrost degradation over 32 years is $z_{2^*} = 3.3(4.8)$ m, and the average degradation rate is $v_* = 10(14.8)$ cm/yr. Parentheses indicate cases with the osmotic effect.

The methane flow through bottom sediments depends on the initial hydrate saturation, which is highly heterogeneous. The experimental value 200 g/(m^2 yr) after 32 years, according to our model, is achieved if the initial hydrate saturation is $S_{h0} = 13(9)\%$, which is reasonable for self-preserved gas hydrates [*Chuvilin et al.*, 2019]. For the initial hydrate saturation value $S_{h0} = 80\%$, which was used as the baseline in the calculations, the flows are significantly higher and decrease to experimental values 200 g/(m^2 yr) only after approximately 1000 years.

Thus, the obtained estimates are in good agreement with the experimental data.

In conclusion, we note that the obtained solution does not account for the greenhouse effect. For relatively long-term predictions, this effect should be considered, as it would significantly accelerate the permafrost degradation process.

The following presents analogous results for the degradation of a frozen layer from below, caused by the heat flux due to the geothermal gradient.

Degradation of hydrate-bearing permafrost from below. As before, the initial conditions are such that the temperature of the layer increases linearly with depth, from 251 K at the upper boundary to 273 K at the lower boundary. The calculations were performed for three different values of the geothermal gradient at the lower boundary of the layer $G = (2.5 \times 10^{-2}; 3 \times 10^{-2}$ and $4 \times 10^{-2})$ K/m. For these values of G, if we take the coefficient of thermal conductivity equal to $\lambda = 2$ W/(m $\cdot$ K), the corresponding heat fluxes are $q = (50; 60$ and $80)$ m W/m^2. These cases are labeled (1, 2, 3). It is assumed that the salinity of the rocks during degradation from below is low and amounts to only 1 g/L [*Frederick and Buffett*, 2014].

Let us consider Figure 7, which corresponds to case 1 ($q = 50$ m W/m^2). This figure is qualitatively similar to Figure 3 for degradation from above, which was described in detail earlier. We note that, as seen in the figure, the rates of frozen layer degradation from below under these conditions are significantly higher than those from above, despite the low salt concentration. This is because, when the heat flux is fixed, the temperature at the boundary increases, whereas during degradation from above, the boundary temperature is fixed. The methane and water fluxes associated with gas hydrate dissociation are also significantly higher during degradation from below, given equal initial hydrate saturations in the rocks.

Figure 8 is qualitatively similar to Figure 4 for degradation from above, showing that osmosis significantly increases pressure and its gradient in the thawed domain.

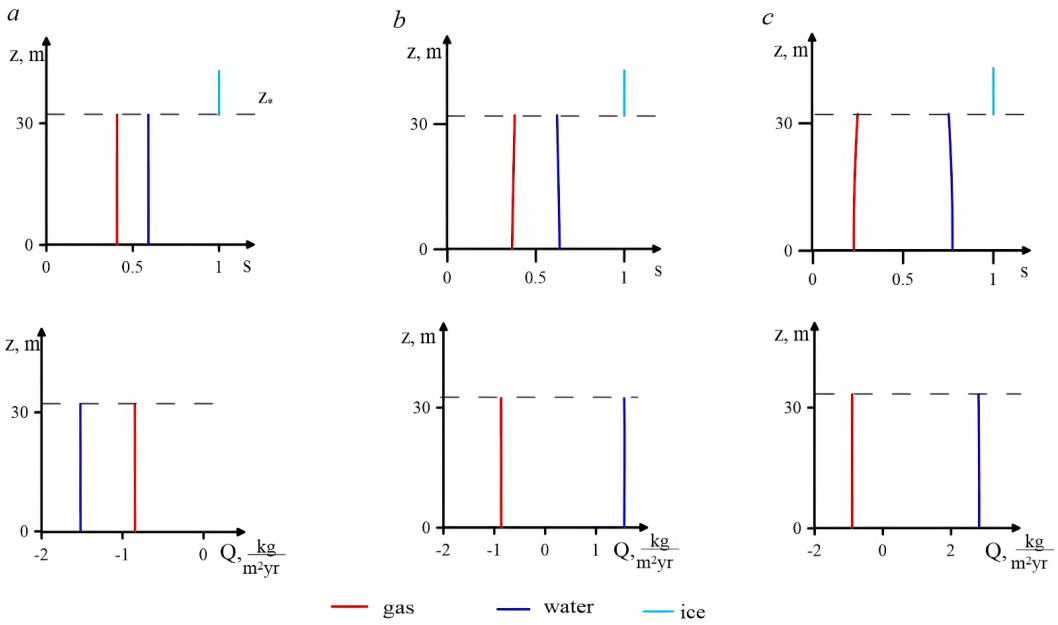

Figure 7. Distributions of pore saturation with different phases in the thawed domain 1000 years after the onset of permafrost degradation, for different values of the osmotic coefficient $\gamma_f = 0$; 10^{-3} and 5×10^{-3} (a, b, c) – top row; mass fluxes of gas and water in the thawed domain after 1000 years – bottom row, for different values of the osmotic coefficient: $\gamma_f = 0$; 10^{-2} and 4×10^{-2} (a, b, c).

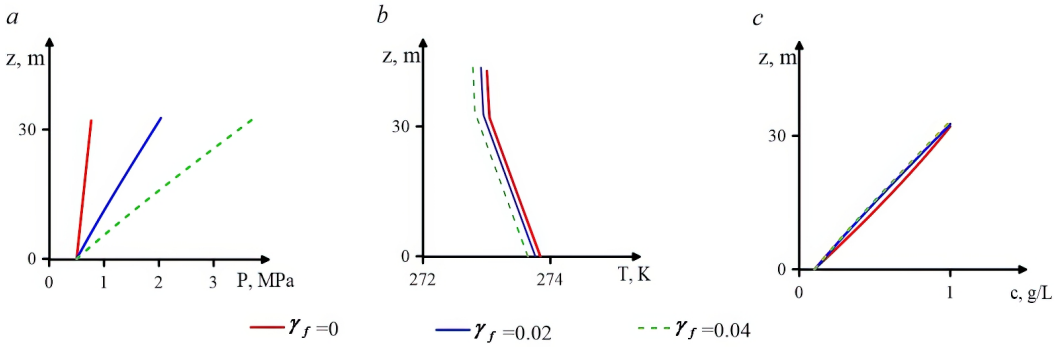

Figure 8. Distributions of pressure (a), temperature (b), and salt concentration (c) with depth 1000 years after the start of the process for various values of the osmosis coefficient: $\gamma_f = 0$; 2×10^{-2} and 4×10^{-2}.

Figure 9a–c shows the dependencies of various parameters on the osmotic coefficient for all three cases 1000 years after the onset of layer degradation. This figure is qualitatively consistent with Figure 5 for degradation from above. Quantitatively, however, it is evident that the degradation rates of the frozen layer from below are significantly higher than those from above, despite the very low salinity of the rocks from below. As for the pressure values near the phase boundary, they are of the same order of magnitude as during degradation from above.

Figure 10 shows the time evolution of various parameters over ten thousand years, with and without the osmotic effect, illustrating their changes from approximately the time of the Arctic shelf marine transgression to the present for all three cases. Solid lines represent cases without osmosis, while dashed lines correspond to cases with an osmotic coefficient of $\gamma_f = 0.1$. Figure 10a–c qualitatively matches Figure 6a–c, described earlier. However, there are significant quantitative differences. Additionally, a key distinction is that the temperature at the lower boundary of the frozen layer increases under a fixed heat flux, whereas the temperature at the upper boundary is fixed. Figure 10d illustrates

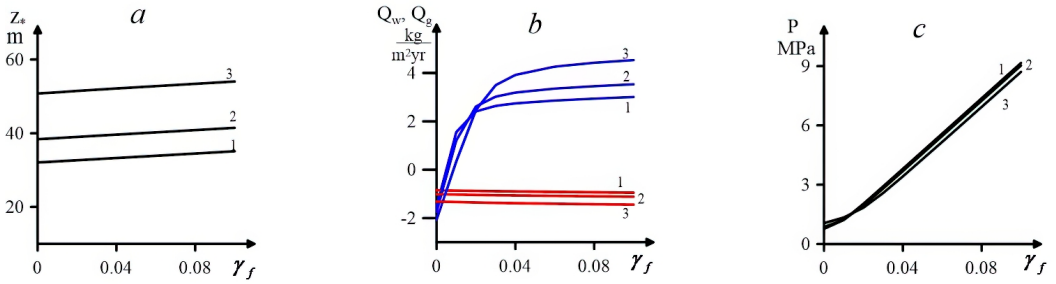

Figure 9. Dependence of the permafrost degradation front (a), mass flux (b), and the pressure at the phase transition boundary (front) (c) on the dimensionless osmotic coefficient 1000 years after the onset of the process. Notation: lines 1 correspond to the case where the heat flow is $q = 50\,\mathrm{m\,W/m^2}$, lines 2 – $q = 60\,\mathrm{m\,W/m^2}$, lines 3 – $q = 80\,\mathrm{m\,W/m^2}$; red lines – gas, blue – water.

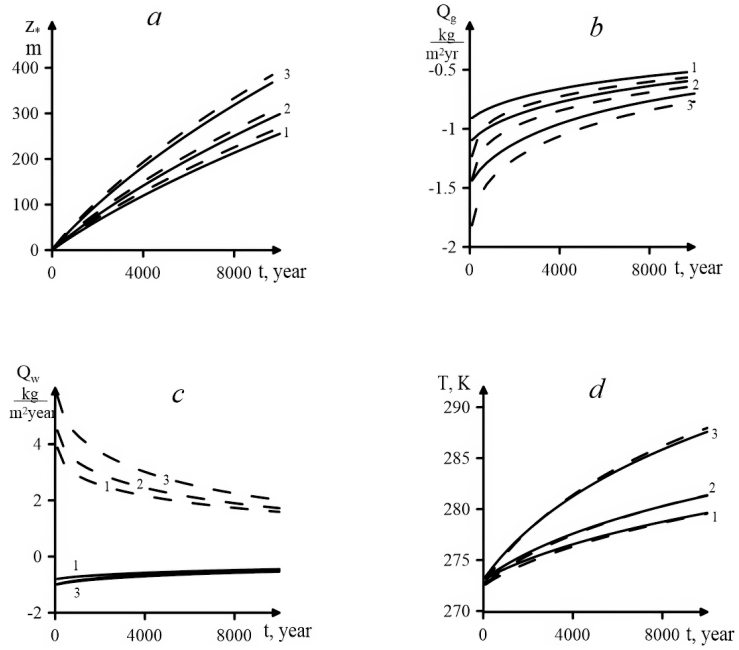

Figure 10. Dependence of the permafrost degradation front from below (a), gas flux (b), water flux (c), and lower boundary temperature (d) on time for all three cases. Notation: lines 1 correspond to the case where the heat flow occurs $q = 50\,\mathrm{m\,W/m^2}$, lines 2 – $q = 60\,\mathrm{m\,W/m^2}$, lines 3 – $q = 80\,\mathrm{m\,W/m^2}$; solid lines correspond to the absence of osmosis, and dotted lines – taking into account the effect of osmosis at $\gamma_f = 0.1$.

the temperature evolution at the lower boundary of the frozen layer when a heat flux is applied.

Table 2. Depth of degradation of hydrate-bearing permafrost from below and gas/water fluxes across the discharge boundary for different heat flux values, with and without the osmotic effect, after 10 000 years. Cases with osmosis at $\gamma_f = 0.1$ are shown in parentheses

$q\left(\mathrm{m\,W/m^2}\right)$	50	60	80
$Z_*\,(m)$	255(269)	299(313)	377(394)
$Q_g\left(\frac{\mathrm{kg}}{\mathrm{m^2\cdot yr}}\right)$	−0.515(−0.558)	−0.59(−0.64)	−0.701(−0.77)
$Q_w\left(\frac{\mathrm{kg}}{\mathrm{m^2\cdot yr}}\right)$	−0.45(1.59)	−0.534(1.724)	−0.478(2.013)

Table 2 presents the final values after 10 000 years, corresponding to Figure 10a–c. This table is similar to Table 1. A comparison of the tables confirms that the degradation rates of the layer and gas hydrates from below are significantly higher than those from above, even with the high salinity of the upper rocks.

Conclusion

A mathematical model has been developed for the degradation of a frozen hydrate-bearing layer, occurring from above due to a sharp temperature increase (marine transgression) and the influence of a saline solution with osmotic effect, and from below due to the heat flux caused by the geothermal gradient. Multivariate calculations were performed. It is shown that permafrost degradation from above occurs even at subzero Celsius temperatures, albeit very slowly, due to the influence of salt. In this case, over ten thousand years, with $T^0 = 272\,\mathrm{K}$ and no osmosis, the degradation front advances only a few meters. However, osmosis can significantly accelerate the process, increasing the degradation depth by a factor of 6–7. For positive temperatures at the upper boundary of the layer, the degradation rate can increase by orders of magnitude compared to subzero temperatures, reaching approximately 100 meters in 10 000 years. In this case, the relative contribution of osmosis is significantly smaller. The contribution of salt at $T^0 = 274\,\mathrm{K}$ is roughly equal to that of temperature, while at $T^0 = 272\,\mathrm{K}$, it even significantly exceeds the impact of temperature. The obtained results are in good agreement with field and experimental data.

When permafrost degrades from below due to heat flux, the degradation rate increases several times, reaching 300–400 meters over 10 000 years. As a result, gas and water fluxes also increase proportionally, given the same hydrate saturation levels.

The study showed that degradation from above follows a slow, approximately square-root law of dependence on time, while degradation from below follows a faster, in the limit nearly linear dependence at long times.

Acknowledgments. The research was funded by the Ministry of Science and Higher Education of the Russian Federation (state assignment No. 075-00269-25-00) and the Russian Science Foundation (grant No. 22-67-00025).

References

Are F. E., Grigoriev M. N., Hubberten H.-W., et al. Comparative shore face evolution along the Laptev Sea coast // Polarforschung. — 2000. — Vol. 70. — P. 135–150.

Arzhanov M. M., Malakhova V. V. and Mokhov I. I. Modeling thermal regime and evolution of the methane hydrate stability zone of the Yamal peninsula permafrost // Permafrost and Periglacial Processes. — 2020. — Vol. 31, no. 4. — P. 487–496. — https://doi.org/10.1002/ppp.2074.

Bogoyavlensky V. I. Fundamental aspects of the catastrophic gas blowout genesis and the formation of giant craters in the Arctic // Arctic: Ecology and Economy. — 2021. — Vol. 11, no. 1. — P. 51–66. — https://doi.org/10.25283/2223-4594-2021-1-51-66. — (In Russian).

Chuvilin E., Ekimova V., Bukhanov B., et al. Role of Salt Migration in Destabilization of Intra Permafrost Hydrates in the Arctic Shelf: Experimental Modeling // Geosciences. — 2019. — Vol. 9, no. 4. — P. 188–206. — https://doi.org/10.3390/geosciences9040188.

Frederick J. M. and Buffett B. A. Taliks in relict submarine permafrost and methane hydrate deposits: Pathways for gas escape under present and future conditions // Journal of Geophysical Research: Earth Surface. — 2014. — Vol. 119, no. 2. — P. 106–122. — https://doi.org/10.1002/2013jf002987.

Harrison W. D. and Osterkamp T. E. A Coupled Heat and Salt Transport Model for Subsea Permafrost. — Geophysical Institute Report No. UAG R-247, University of Alaska, 1976.

Istomin V. A. and Yakushev V. S. Gas Hydrates in Natural Conditions. — Moscow : Nedra, 1992. — 235 p. — EDN: YSOMOR ; (in Russian).

Kizyakov A., Zimin M., Sonyushkin A., et al. Comparison of Gas Emission Crater Geomorphodynamics on Yamal and Gydan Peninsulas (Russia), Based on Repeat Very-High-Resolution Stereopairs // Remote Sensing. — 2017. — Vol. 9, no. 10. — P. 1023. — https://doi.org/10.3390/rs9101023.

Lobkovskii L. I., Nikiforov S. L., Shakhova N. E., et al. Mechanisms responsible for degradation of submarine permafrost on the eastern arctic shelf of Russia // Doklady Earth Sciences. — 2013. — Vol. 449, no. 1. — P. 280–283. — https://doi.org/10.1134/S1028334X13030124.

Lobkovsky L. I., Baranov A. A., Ramazanov M. M., et al. Possible Seismogenic-Trigger Mechanism of Methane Emission, Glacier Destruction and Climate Warming in the Arctic and Antarctic // Izvestiya, Physics of the Solid Earth. — 2023. — Vol. 59, no. 3. — P. 364–376. — https://doi.org/10.1134/s1069351323030084.

Lobkovsky L. I. and Ramazanov M. M. Thermomechanical Waves in the Elastic Lithosphere-Viscous Asthenosphere System // Fluid Dynamics. — 2021. — Vol. 56, no. 6. — P. 765–779. — https://doi.org/10.1134/s0015462821060100.

Lobkovsky L. I., Ramazanov M. M., Semiletov I. P., et al. Mathematical Model of the Decomposition of Unstable Gas Hydrate Accumulations in the Cryolithozone // Geosciences. — 2022. — Vol. 12, no. 9. — P. 345. — https://doi.org/10.3390/geosciences12090345.

Malakhova V. V. and Golubeva E. N. Estimation of the permafrost stability on the East Arctic shelf under the extreme climate warming scenario for the XXI century // Ice and Snow. — 2016. — Vol. 56, no. 1. — P. 61–72. — https://doi.org/10.15356/2076-6734-2016-1-61-72. — (In Russian).

Morgado A. M. O., Rocha L. A. M., Cartwright J. H. E., et al. Osmosis Drives Explosions and Methane Release in Siberian Permafrost // Geophysical Research Letters. — 2024. — Vol. 51, no. 18. — e2024GL108987. — https://doi.org/10.1029/2024gl108987.

Neuzil C. E. Osmotic generation of 'anomalous' fluid pressures in geological environments // Nature. — 2000. — Vol. 403, no. 6766. — P. 182–184. — https://doi.org/10.1038/35003174.

Osterkamp T. A. Sub-sea Permafrost // Encyclopedia of Ocean Sciences / ed. by J. Steele, K. Turekian and S. Thorpe. — Massachusetts : Elsevier, 2001. — P. 559–569. — https://doi.org/10.1016/b978-012374473-9.00008-4.

Osterkamp T. E. and Gosink G. P. Variations in permafrost thickness in response to changes in paleoclimate // Journal of Geophysical Research: Solid Earth. — 1991. — Vol. 96, B3. — P. 4423–4434. — https://doi.org/10.1029/90jb02492.

Ramazanov M., Bulgakova N. and Lobkovsky L. Mathematical Model of Freezing of Rocks Saturated With Salt Solution Taking Into Account the Influence of Osmosis // Russian Journal of Earth Sciences. — 2023. — Vol. 23, no. 5. — ES5007. — https://doi.org/10.2205/2023es000857.

Ramazanov M. M. Mathematical Model of Filtration of Solutions in a Porous Medium with Semipermeable Inclusions. Osmotic Convection // Journal of Engineering Physics and Thermophysics. — 2023. — Vol. 96, no. 3. — P. 823–833. — https://doi.org/10.1007/s10891-023-02744-7.

Ramazanov M. M., Bulgakova N. S., Gadzhimagomedova S. R., et al. Nonlinear Problem of Filtration Convection of a Salt Solution Caused by the Osmotic Effect // Journal of Applied Mechanics and Technical Physics. — 2025a. — Vol. 66, no. 1. — P. 32–44. — https://doi.org/10.1134/s0021894425010122.

Ramazanov M. M., Bulgakova N. S., Lobkovsky L. I., et al. Dissociation Kinetics of Methane Hydrate in Frozen Rocks under Decreasing External Pressure: Mathematical and Experimental Modeling // Doklady Earth Sciences. — 2024a. — Vol. 516, no. 2. — P. 1028–1035. — https://doi.org/10.1134/s1028334x24601391.

Ramazanov M. M., Bulgakova N. S. and Lobkovsky L. I. Mathematical Criterion for the Formation of Cryopags during the Freezing of Rocks Saturated with Salt Solution // Doklady Rossijskoj akademii nauk. Fizika, tehničeskie nauki. — 2024b. — Vol. 515, no. 2. — P. 59–66. — https://doi.org/10.31857/s2686740024020094. — (In Russian).

Ramazanov M. M., Bulgakova N. S. and Lobkovsky L. I. Degradation patterns of hydrate-containing permafrost rocks: modeling taking into account the osmotic effect // Prikladnaya mekhanika i tekhnicheskaya fizika. — 2025b. — 4(392). — P. 129–143. — https://doi.org/10.15372/PMTF202415575. — (In Russian).

Ramazanov M. M., Karakin A. V. and Lobkovskiy L. I. Mathematical Model for the Motion of Solutions Taking into Account the Osmotic Effect // Doklady Earth Sciences. — 2019. — Vol. 489, no. 1. — P. 1306–1309. — https://doi.org/10.1134/s1028334x19110060.

Romanovskii N. N., Hubberten H.-W., Gavrilov A. V., et al. Offshore permafrost and gas hydrate stability zone on the shelf of East Siberian Seas // Geo-Marine Letters. — 2005. — Vol. 25, no. 2/3. — P. 167–182. — https://doi.org/10.1007/s00367-004-0198-6.

Ruppel C. D. Methane hydrates and contemporary climate change // Nature Education Knowledge. — 2011. — Vol. 3, no. 10.

Semiletov I. P. and Shakhova N. E. Greenhouse gases balance and climate change: Role of permafrost degradation in the Arctic // Vestnik of the Far East Branch of the Russian Academy of Sciences. — 2024. — 4(236). — P. 5–43. — https://doi.org/10.31857/S0869769824040015. — EDN: IRWLDY ; (in Russian).

Sergienko V. I., Lobkovskii L. I., Semiletov I. P., et al. The degradation of submarine permafrost and the destruction of hydrates on the shelf of east arctic seas as a potential cause of the "Methane Catastrophe": some results of

integrated studies in 2011 // Doklady Earth Sciences. — 2012. — Vol. 446, no. 1. — P. 1132–1137. — https://doi.org/10.1134/s1028334x12080144.

Shakhova N., Semiletov I., Gustafsson O., et al. Current rates and mechanisms of subsea permafrost degradation in the East Siberian Arctic Shelf // Nature Communications. — 2017. — Vol. 8, no. 1. — https://doi.org/10.1038/ncomms15872.

Shakhova N., Semiletov I., Salyuk A., et al. Geochemical and geophysical evidence of methane release over the East Siberian Arctic Shelf // Journal of Geophysical Research: Oceans. — 2010. — Vol. 115, no. C8. — P. C08007. — https://doi.org/10.1029/2009jc005602.

Streletskaya I. D. and Leibman M. O. Cryogeochemical interrelation of massive ground ice, cryopegs, and enclosing deposits of Central Yama // Kriosfera Zemli. — 2002. — Vol. 6, no. 3. — P. 15–24. — (In Russian).

Tsypkin G. G. Flows with Phase Transitions in Porous Media. — Moscow : Fizmatlit, 2009. — 232 p. — (In Russian).

Vasiliev V. I., Maksimov A. M., Petrov E. E., et al. Heat and Mass Transfer in Freezing and Thawing Soils. — Moscow : Nauka, 1996. — 224 p. — (In Russian).

Yakushev V. S. Natural gas and gas hydrates in permafrost. — Moscow : VNIIGAZ, 2009. — 192 p. — EDN: OTRYFK ; (in Russian).

Yakushev V. S., Gafarov N. A., Karnaukhov S. M., et al. Gas hydrates in the Arctic and the World Ocean: features of occurrence and development prospects. — Moscow : Nedra, 2014. — 251 p. — EDN: VNKPSF ; (in Russian).